

# The physical oceanography of Jones Bank: A mixing hotspot in the Celtic Sea



Matthew R. Palmer<sup>a,\*</sup>, Mark E. Inall<sup>b</sup>, Jonathan Sharples<sup>a,c</sup>

<sup>a</sup> National Oceanography Centre, 6 Brownlow Street, Liverpool L3 5DA, UK

<sup>b</sup> Scottish Association for Marine Science (SAMS), Oban, Argyll PA37 1QA, UK

<sup>c</sup> School of Environmental Sciences, University of Liverpool, Liverpool L69 3GP, UK

## ARTICLE INFO

### Article history:

Available online 26 June 2013

## ABSTRACT

New measurements are presented of the currents and hydrography at Jones Bank in the Celtic Sea. These measurements, collected during the summer of 2008, identify a highly energetic internal wavefield generated by the local interaction of seasonally stratified flow with topography. Observations close to the bank crest reveal internal waves of up to 40 m amplitude; approaching 50% of the local water depth. These waves occur during spring periods and are predominantly associated with off-bank tidal flow. We provide evidence that these waves are the result of hydraulic control of the tidal currents which result in supercritical flow in the bottom mixed layer (bml) on the upper slopes of the bank. The waning tide produces a transition from super to subcritical flow, identifiable as a regular hydraulic jump on the bank slope. Microstructure measurements identify a turbulent 'bore' associated with such jumps that increases bml turbulence by several orders of magnitude and produces a regular burst of enhanced mixing at the base of the ever-present thermocline. Additional mixing in the surface mixed layer is provided during gale force conditions during the first of the two spring tides observed, occurring at the start of our three-week measurement period. The average thermocline mixing rate during *stormy spring* tide conditions is  $1.9 (\pm 1.0, 95\%) \times 10^{-3} \text{ m}^2 \text{ s}^{-1}$ , driven by both surface mixing and hydraulic jumps. During the later *calm spring* period the average thermocline mixing rate is  $3.3 (\pm 1.7) \times 10^{-4} \text{ m}^2 \text{ s}^{-1}$ , dominated by jump associated events. By comparison, the intervening neap tide period produces no hydraulic jumps and is characterised by relatively calm weather. A strong shear layer is however maintained during this 'quiet' period sufficient to enhance thermocline turbulence by a factor 1000 above background levels. A short lived peak in thermocline turbulence during the neap period produces diapycnal mixing as high as  $1.6 \times 10^{-2} \text{ m}^2 \text{ s}^{-1}$  however a more representative 'background' thermocline mixing rate is  $2.8 (\pm 0.6) \times 10^{-5} \text{ m}^2 \text{ s}^{-1}$ .

© 2013 The Authors. Published by Elsevier Ltd. Open access under [CC BY-NC-ND license](https://creativecommons.org/licenses/by-nc-nd/4.0/).

## 1. Introduction

Despite the relatively small spatial scale of shelf seas when compared to the open ocean they have been shown to be disproportionately significant to biological production and subsequently carbon sequestration (e.g. Muller-Karger et al., 2005; Tsunogai et al., 1999). Of primary importance to the biological success of shelf seas is the ready availability of nutrients when compared to the open ocean. The physical mechanisms that control the biogeochemical pathways on shelf seas are however still under discussion. The dynamics of the spring bloom are understood (Fasham et al., 1983; Sambrotto et al., 1986) and account for much of the initial uptake of nutrients during the transition from the generally well mixed winter months to the onset of seasonal stratification which affects large areas of temperate shelf seas. There remains

however a relatively weak but significant level of primary production throughout the seasonally stratified periods that appears ubiquitous over the stratified ocean, identified as a subsurface chlorophyll maximum (SCM) (Anderson, 1969; Pingree et al., 1982). The maintenance of the SCM is dependent on the relative stability and light availability of the seasonal pycnocline coupled with a vertical exchange of nutrients from the typically rich lower layers into the pycnocline where a resource starved phytoplankton community are quick to assimilate any available nutrients (Sharples and Tett, 1994).

A variety of mechanisms have been implicated in pycnocline fluxes in shelf seas. The primary candidate mechanism is the breaking of internal waves most often generated by a transfer of energy from the barotropic tide through the interaction of stratified flow with topography. Some of the most dramatic and energetic examples are internal waves generated at the shelf break (Pingree et al., 1981; Sandstrom and Elliott, 1984; Carter et al., 2005) and the transfer of energy by non-linear solitons away from

\* Corresponding author. Tel.: +44 1517954800.

E-mail address: [matthew.palmer@noc.ac.uk](mailto:matthew.palmer@noc.ac.uk) (M.R. Palmer).

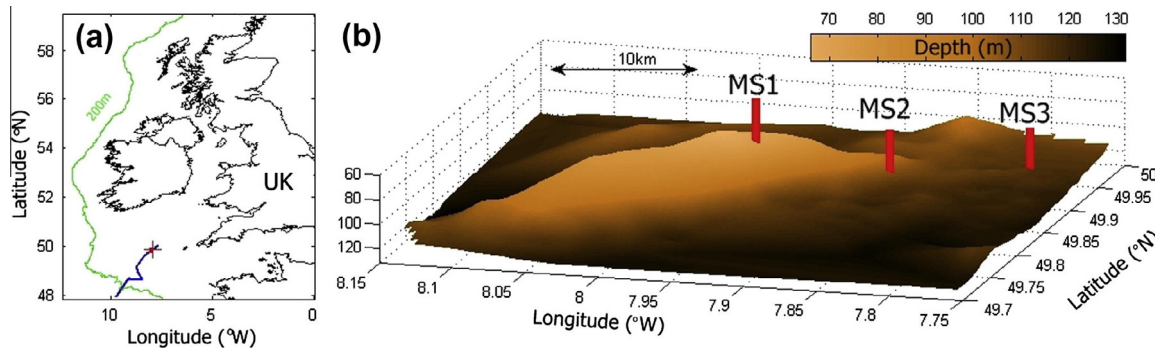


**Fig. 1.** (a) Map showing the location of Jones Bank (red cross) and the path of the Scanfish transect (blue line). The approximate location of the shelf break is indicated by the 200 m depth contour (green line). (b) The topography over and around the bank is derived from the data collected using the ship's echo sounder during the experiment. The positions of the three stations MS1, MS2 and MS3 (west to east) are indicated by the red vertical lines. (For interpretation of the references to color in this figure legend, the reader is referred to the web version of this article.)

the break region into the open ocean (Pingree et al., 1986) and onto the shelf (Rippeth and Inall, 2002). The vast majority of baroclinic energy has been shown to be dissipated close to the generation region, within a few tens of kilometers (e.g. Pingree et al., 1986; Holloway et al., 2001). A common hypothesis is that the remaining energy is capable of penetrating the full breadth of the shelf, explaining the ubiquity of internal waves in stratified shelf seas (e.g. Rippeth and Inall, 2002; MacKinnon and Gregg, 2003) and thus providing an internal mixing mechanism sufficient to maintain the SCM by providing a low but persistent level of turbulent energy available for mixing at the thermocline. More recent studies have suggested that the baroclinic energy at the shelf break may have little or no influence on internal mixing deep on the shelf. Green et al. (2008) showed that rather than providing a simple 2-dimensional wave generator the complexity of the Celtic Sea shelf slope produces an equally complex internal wavefield that results in only a weak on-shelf flux of baroclinic energy and a net flux perpendicular to the shelf edge.

Further potential mixing mechanisms have been identified in the proximity of topographic features on the shelf. A few shelf sea banks have been investigated; Brickman and Loder (1993) identified the interaction of stratified flow with Georges Bank produced hydraulic jumps on each phase of the tide, Hibiya (1988) similarly identified tidally generated internal waves at Stellwagen Bank and Nash and Moum (2001) identified intense mixing associated with hydraulic jumps due to a slope driven jet being forced over Stonewall Bank. Studies 300 km on the European shelf by Palmer et al. (2008) showed that despite the continued presence of an internal wavefield and a weak level of mixing sufficient to maintain a steady vertical flux of nutrients, there was no evidence of energy propagating from the shelf break or other nearby topographic features. Furthermore analysis presented separately in this volume (Inall et al., 2013) indicates that internal tidal energy derived at the shelf break has largely been dissipated at the location of Jones Bank, some 250 km 'on shelf'. It has been suggested alternatively that vertical mixing far from the shelf break is instead due to the weak but regular availability of energy from wind driven inertial oscillations which maintain a high shear region in the pycnocline that is only marginally stable (Palmer et al., 2008). Such a state of marginal stability has been identified in other shelf sea studies away from regions of extreme topography (Rippeth et al., 2005; MacKinnon and Gregg, 2003; van Haren, 2000). In a marginal state, mixing becomes likely when even weak secondary processes are available such as a low energy internal wavefield, wind mixing or convective instability from surface cooling (Palmer et al., 2008).

In this paper we present a new series of measurements made over Jones Bank in the Celtic Sea during the summer of 2008 (Fig. 1). The Celtic Sea and the remainder of the European conti-

ental shelf is separated from the deep ocean by a rapidly descending shelf break and is strongly stratified over much of its interior throughout the summer months. Jones Bank is situated over 200 km east of the nearest shelf slope and approximately 100 km west of the English mainland. Jones Bank is shallow sloping and low profile, rising 30 m over its 50 km long major axis in approximately 130 m of surrounding sea. The bank forms part of an extensive field of southwest–northeast orientated banks, identified as discrete sand bodies resting on paleotopographic features formed during the last glacial retreat (Scourse et al., 2009). As such Jones Bank is representative of many of the banks that litter European shelf seas. The closest known topographic features of comparable size are Labadie bank and North West bank located ~50 km to the north and northwest.

Our measurements will be used to describe the physical oceanography of Jones Bank and identify the influence of this modest topographic feature on the stratified tidal flow. From our direct measurements of the dissipation rate,  $\epsilon$ , of the turbulent kinetic energy (TKE) we describe the temporal evolution of mixing over the bank and quantify the vertical mixing rate at the pycnocline during spring and neap periods. These long-term observations of a 'typical' and shallow sloping shelf sea bank are unique as they present the regular interaction of seasonally stratified tidal flow with topography and the spatial variability of mixing mechanisms over shelf sea banks. As such these data provide an important insight into the physical maintenance of the shelf sea SCM. Section 2 presents the instrumentation and experimental design. Section 3 presents the results of our study to describe the general hydrography over the bank (3.1), provide an overview of data from each mooring site (3.2), examine the role of internal waves and shear (3.3), present the vertical and temporal evolution of turbulence (3.4), investigate the role of hydraulic jumps (3.5) and finally present estimates of turbulent mixing (3.6). Results are summarised in Section 4 and our conclusions are presented in Section 5 with a discussion of our findings.

## 2. Methods

Instrumentation was deployed at 3 sites on Jones Bank for 19 days from the 5th July to 24th July 2008. Three sites were chosen situated on the northwest slope along the line of the longest axis of the bank (Fig. 1). The sites were evenly spaced 10 km apart from a near crest station (MS1), on the bank slope (MS2) and at the base of the slope (MS3). Near identical arrays of instruments were deployed at the each of the three bank stations; each mooring consisted of a bedframe mounted RDI 300 kHz acoustic Doppler current profiler (ADCP) which recorded along beam velocities at 1 Hz with a depth resolution of 2 m (MS1), 2 m (MS2) and 4 m

(MS3). Horizontal velocities were calculated from recorded radial velocities using the methods described by Lu and Lueck (1999). Current velocities were subsequently resolved from the near bed to within a few metres of the sea surface. Vertical shear of horizontal currents was calculated as the difference in velocity between subsequent measurements scaled by the measured depth resolution. A vertical chain of thermistors was moored at each station recording temperature every minute and every 2 m in the upper half of the water column and every 5 m at greater depths. Pressure sensors were placed at a variety of points along each thermistor chain to allow for positional correction due to straining.

All three thermistor chains successfully recorded data for the majority of the deployment duration. The density field at Jones Bank was predominately controlled by temperature that accounted for 99.75% of the observed variance in density. Due to the abundance of temperature data from moored and profiling instrumentation temperature will therefore be used as a proxy for density throughout this paper.

Unfortunately failures occurred in the ADCPs deployed at MS2 and MS3. The reason for failure appeared identical in both instruments and was identified to be the result of an unsuccessful transfer to a second flash memory card. The resultant measurement period for the slope and off bank ADCP was near identical, both failing one week after deployment on the 12th July 2008. The ADCP at MS1 successfully recorded velocity data for the entire deployment period and will thus be used to describe much of the current structure over the bank. From these data we calculated the barotropic tidal velocity from the depth mean and the baroclinic velocity as the residual i.e. depth mean removed. While this follows common convention (e.g. Rippeth and Inall, 2002; MacKinnon and Gregg, 2003) the depth mean currents may include some non-tidal components due to flow interaction with the bank and meteorological contributions. The attempted removal of such contributions is however likely to introduce further error to the baroclinic velocity estimate so depth mean removed is used as a 'best estimate'.

The availability of coincident vertical profiles of current velocity and density (temperature) permits investigation of the relative contribution to the flow energy from its kinetic and potential components. Within a two-layer, stratified flow (which describes much of the summer stratified NW European shelf (Pingree et al., 1978; Elliott and Clarke, 1991) the relative contribution to the flow from each component can be examined using the non-dimensional, composite internal Froude number (Armi, 1986);

$$G^2 = F_1^2 + F_2^2$$

where

$$F_i^2 = \frac{u_i^2}{g'h_i}, \quad g' = g \frac{\Delta\rho}{\rho} \quad (1)$$

where  $F_i$  are the internal densimetric Froude numbers for upper ( $i = 1$ ) and lower ( $i = 2$ ) layers of thickness  $h_i$  calculated using the reduced gravitational acceleration,  $g'$ , derived from the density difference between those layers,  $\Delta\rho$ . Where  $G^2 > 1$  flow is dominated by its kinetic energy and is termed *supercritical* and the flow is considered to be under hydraulic control. A consequence of this state is that waves generated at the interface are unable to travel against the flow. During subcritical states ( $G^2 < 1$ ) potential energy dominates and waves are free to propagate in any direction. Individual layers are deemed supercritical where  $F_i > 1$ . The transition between supercritical and subcritical hydraulic states may occur rapidly as a hydraulic jump (Farmer and Armi, 1999). Such jumps have been observed to promote turbulent mixing (e.g. Moum and Nash, 2000) and subsequently a local loss of energy. Also, during periods of hydraulic control accelerated flows in individual layers may

increase interfacial shear and promote mixing through shear instability (Lawrence, 1990). From (1) it is clear that a change in hydraulic state may occur whenever there is either a change in flow (e.g. from oscillatory tidal currents) or layer thickness (through flow interaction with topographic features).

In addition to the moored instrumentation deployed in the experiment microstructure measurements were made with a VMP750 turbulence profiler manufactured by Rockland Scientific International (<http://www.rocklandscientific.com>). The instrument is tethered to a manually operated winch mounted at the ship's stern. To prevent entanglement in the ship's rudder or propeller and to maintain a profiling position close to the relevant location, the ship maintained a constant  $\sim 0.5$  kts through-water speed throughout operations. The instrument is deployed with a loose tether such that it is free-falling and unlikely to be affected by the physical influence of the ship. During descent the instrument records shear, temperature and conductivity microstructure at 512 Hz and temperature and conductivity from the auxiliary Seabird sensors are recorded at 16 Hz. On collision with the seabed the instrument is recovered to the surface when it can be redeployed or recovered. Vertical measurement limits are set by the time taken for the instrument to fall beneath the ship's wake, reach an optimal fall speed ( $0.6 \text{ ms}^{-1} < w < 0.8 \text{ ms}^{-1}$ ) and the need to protect the probe sensors from collision with the seabed. With the use of a probe guard, measurements were typically made between 8 m depth and 15 cm above the seabed. The capability of this instrument to measure so close to the bed permits almost complete coverage of benthic boundary layer turbulence and will enable the separation of mixing mechanisms and permit direct calculation of bed stress in this study. Typical fall speeds of  $\sim 0.7 \text{ ms}^{-1}$  resulted in a single vertical profile being achieved in approximately 3 min with a similar time required for recovery to the surface.

The dissipation rate of turbulent kinetic energy,  $\varepsilon$ , is determined through integration of the velocity shear spectrum (Tennekes and Lumley, 1972),

$$\varepsilon = \frac{15}{2} \nu \overline{\left(\frac{\partial u'}{\partial z}\right)^2} \quad (\text{W/kg}) \quad (2)$$

where  $\nu$  is the kinematic viscosity of seawater and the bracketed term is the variance in the vertical gradient of turbulent fluctuations in horizontal velocity measured by the shear microstructure probes, the overbar denotes a spatial average (Oakey, 1982). The extent of the inertial sub-range that the shear probe is able to measure is limited; resolvable turbulent eddies are restricted by the size of the instrument ( $\sim 2$  m) and that of the sensitive section of the probe ( $\sim 5$  mm) and energy levels are restricted by instrument noise and attenuation due to spatial averaging. To account for energy loss due to the latter, spectra were 'boosted' using the methods of Macoun and Lueck (2004) and estimates of  $\varepsilon$  were increased to include unresolved wavenumbers based on the idealised turbulent spectrum suggested by Nasmyth (1970).  $\varepsilon$  was calculated over 4 s, 50% overlapping vertical sections which results in a vertical resolution of approximately 1.4 m.

To understand the consequences of this turbulence on the local rate of mixing we can estimate a vertical eddy diffusion rate,  $K_z$ , by considering the competition between mixing energy, represented by  $\varepsilon$ , and buoyant production of TKE represented by the buoyancy frequency,  $N^2$ ,

$$K_z = \Gamma \frac{\varepsilon}{N^2} \quad (3)$$

and  $\Gamma$  is a mixing efficiency which we will assume to be a constant fraction of 0.2 (Osborn, 1980) but has been suggested to fall somewhere between 0.15 and 0.2 by other authors (e.g. Moum, 1996; Ivey and Imberger, 1991).

Three time series of  $\varepsilon$  were made with the VMP750 at site MS2 (Fig. 1):

1. A single tidal ( $M_2$ ) cycle collected between 14:44 6th July and 02:59 7th July 2008.
2. A single tidal ( $M_2$ ) cycle, 11:55 14th July and 00:10 15th July 2008.
3. Two tidal ( $M_2$ ) cycles, 07:57 21st July and 09:24 22nd July 2008.

The decision to concentrate microstructure measurements at the mid-slope station was based on previous observations which had identified a persistent chlorophyll maximum in the thermocline at this location and regularly enhanced internal mixing associated with off-bank flow (Tweddle et al., 2013).

### 3. Results

#### 3.1. General hydrography

Data from the across shelf Scanfish survey (Fig. 2) provide a valuable and rare snapshot of the physical structure of ocean

density and the distribution of chlorophyll over a summer stratified shelf sea. The transect also provides the first indicators of vertical mixing; the variability in topography is mirrored by dramatic changes in the position and thickness of the pycnocline, steep slopes are associated with rapid horizontal changes in pycnocline depth indicative of internal waves and a more diffuse vertical distribution of density is suggestive of localised mixing (Rippeth, 2005). In contrast to the apparently energetic environment associated with the undulating topography that covers the first 120 km of the transect, flat regions of the shelf are characterised by a more quiescent and regular density distribution. Chlorophyll abundance over the shelf is equally divisible, with highly variable, patchy concentration over regions of rough topography and more regularly distributed but weaker concentration over the smoother on-shelf regions. Compared to the rapidly changing vertical structure around the shelf break, Jones Bank appears relatively stable during the observed period with a near even distribution of high density chlorophyll over the extent of the bank and up to 40 km upstream, (200 km in Fig. 2c). The vertical flux of nutrients required to maintain this SCM during summer months (Sharples et al., 2001) provides a biological indicator of vertical mixing at the base of the

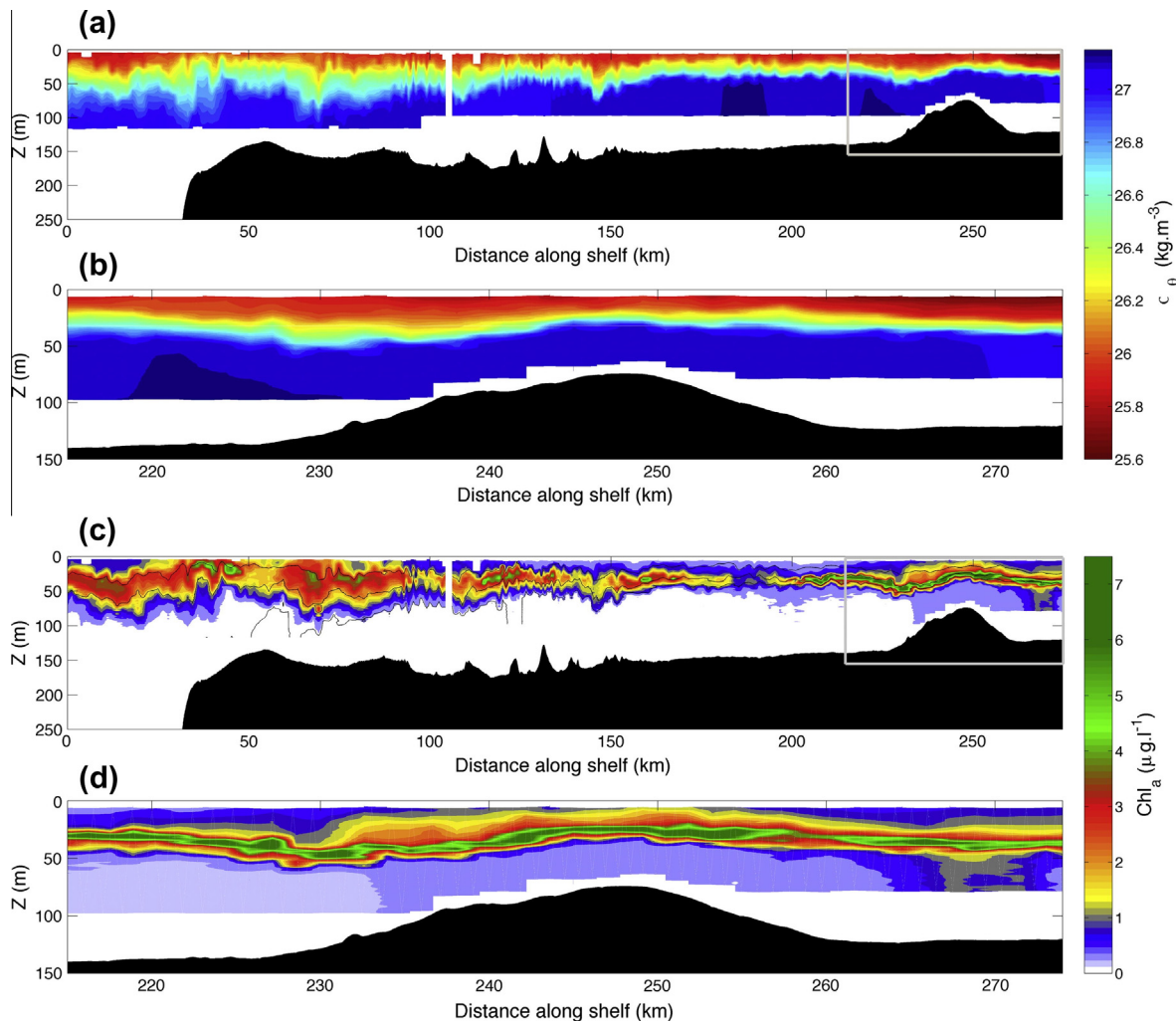


**Fig. 2.** Scanfish provides a high resolution picture of the vertical and horizontal structure of density (a) and chlorophyll (c) distribution over the continental shelf from beyond the shelf break to within 50 km of the English coast. The transect was undertaken between 23:15 25th July and 18:40 26th July 2008 travelling at approximately 9 kts, undulating vertically between 5 m and 120 m depth. The on shelf end (right) of the transect passes over Jones Bank (shown by the grey rectangles in (a) and (b)) and are shown in subsections in (c) and (d). (c) The vertical density structure over the bank was highly stable although weak horizontal gradients were evident in the bottom mixed layer (bml) indicative of enhanced mixing. A persistent but highly variable chlorophyll maximum was associated with the pycnocline region. Horizontally, maxima are observed in close proximity of topographic features with the highest observed concentration of chlorophyll identified over and around Jones Bank (d). A small increase in bml chlorophyll is evident at the NE extent of the transect, close to the bank.

pycnocline. The pycnocline is displaced vertically over the extent of Jones Bank with an apparent wavelength of similar magnitude to the horizontal scale of the feature. On closer inspection there is evidence of an intrusion of chlorophyll into the bottom mixed layer over the bank region, and more distinctly, 10 km east of the bank slope (Fig. 2d). The existence of elevated levels of chlorophyll in the bottom mixed layer may be assumed as a second biological indication of enhanced vertical mixing at the pycnocline as sub-thermocline conditions are insufficient to sustain primary production. Detailed analyses of the internal wave energetics of this Scanfish section are reported elsewhere in this volume (Inall et al., 2013).

Wind data from the ship's meteorological sensors (Fig. 4a) does not include the uncomfortable force 9 ( $>22 \text{ ms}^{-1}$ ) gales encountered during transit to the mooring positions. However, some of the consequences of the gale are clearly evident in the more diffuse nature of the thermocline (Fig. 4b) during the first 5 days of the mooring deployment when compared to the remaining period. Steadily decreasing west to north-westerly winds followed the gale for approximately one week during the transition from spring to neap tides. Although no further gale force conditions were experienced, winds in excess of  $5 \text{ ms}^{-1}$  were encountered throughout the majority of the experiment except and a short period of calm during the second spring tide towards the end of deployment.

Surface layer temperature (Fig. 4b) was seen to rise steadily from  $14^\circ\text{C}$  on the 5th July to a little over  $16.5^\circ\text{C}$  on the 24th July equivalent to a decrease in surface density of  $\sim 0.56 \text{ kg m}^{-3}$ . Near bed temperatures varied little during the course of the experiment maintaining a mean around  $10.6^\circ\text{C}$  although a fluctuation of up to  $0.15^\circ\text{C}$  was associated with tidal advection of slightly warmer bottom water. The maintenance of this warm region is indicative of enhanced diapycnal mixing over the top of the bank (Brickman and Loder, 1993) as heat from the sml is mixed downwards. The entire bank region and surrounding area were strongly vertically stratified throughout the deployment. The strength of stratification can be characterised by the buoyancy frequency squared,  $N^2 = g/\rho_0 \cdot (\delta\rho/\delta z)$ . The maximum thermocline stratification (calculated as the highest  $N^2$  value) doubled during the course of the deployment, increasing near linearly from  $N^2 = 5 \times 10^{-4} \text{ s}^{-2}$  to  $1 \times 10^{-3} \text{ s}^{-2}$ .

While it was disappointing that the off-bank ADCP record at MS3 was too short in duration to resolve the spring neap cycle the current velocity was well represented by measurements made at MS1. Barotropic current velocity at the MS1 accounted for 76% of the variance of the week-long measured currents at MS3. The tidal currents were dominated by the semi-diurnal lunar and solar constituents,  $M_2$  and  $S_2$ , which accounted for 93.5% of the variance in depth averaged velocity at MS1 (Table 1). The  $S_2$  component was sufficiently strong to produce a significant spring-neap variation in current magnitude; spring tide peak currents typically exceeding  $0.5 \text{ ms}^{-1}$  and neap tide current maxima was as low as  $0.2 \text{ ms}^{-1}$ . The major axis of the barotropic tide was orientated approximately  $60^\circ\text{N}$  in close alignment with the orientation of the major axis of Jones Bank (Fig. 3). Throughout the paper we shall refer to major axis currents aligned along this frame of reference,

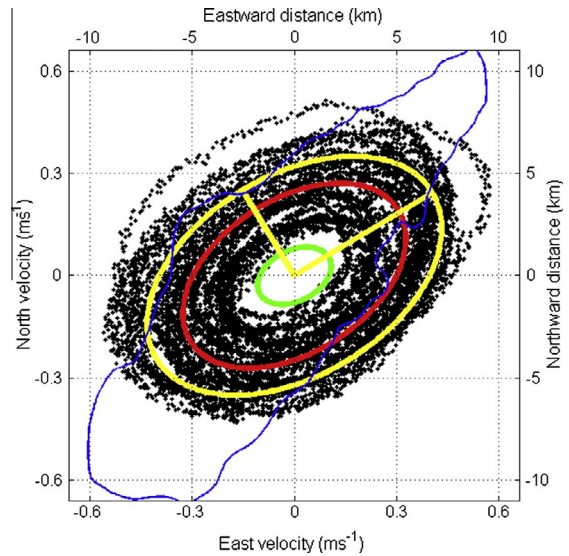


**Fig. 3.** The tidal velocity at MS1 was dominated by the  $M_2$  (red) and  $S_2$  (green) constituents. The combined semi-diurnal ellipse (yellow) is shown alongside the observed depth mean velocity (black, residual removed) for comparison. The major and minor current positive axes directions are indicated (yellow lines). The 120 m isobath is overlaid (blue) to demonstrate the tidal current orientation relative to Jones Bank. (For interpretation of the references to color in this figure legend, the reader is referred to the web version of this article.)

$60^\circ\text{N}$  +ve, and minor axis currents  $330^\circ\text{N}$  +ve. Instantaneous currents are regularly observed to be significantly stronger than barotropic current velocity particularly at the near crest station MS1 where spring tide currents often exceed barotropic flow by over  $0.2 \text{ ms}^{-1}$ , occasionally exceeding  $0.4 \text{ ms}^{-1}$ .

### 3.2. Site-by-site overview

Data from each of the three stations (MS1, MS2, and MS3) are now examined in more detail. Due to the gale force conditions around spring deployment and quiescent winds during the second spring period we are presented with three very different forcing states to compare: (1) *stormy spring*, (2) *windy neap* and (3) *calm spring*. For reference, spring tides occurred on days 186 and 202 (5th and 21st July), neap tides on day 194 (13th July).

#### 3.2.1. MS1: near crest station

Data from both the ADCP and thermistor chain time series show the near crest site MS1 to be a continuously highly active, energetic site (Fig. 4). An energetic internal wavefield is evident throughout the temperature time series with maximum pycnocline displacements approaching 40 min magnitude during spring tides, equivalent to approximately 50% of the local water depth. Energy is spread over a broad waveband but dominated by low mode, low frequency (semi-diurnal) oscillations throughout both spring and the neap periods. Rapid transitions from negative to positive vertical displacements at the thermocline regularly occur during both spring

**Table 1**

The six dominant tidal constituents account for 94.7% of variance in the depth mean velocity at MS1. The semi-diurnal constituents  $M_2$  and  $S_2$  account for 93.5% of that variance.

Tidal Constituent	Major axis amplitude ( $\text{ms}^{-1}$ )	Major axis phase ( $^\circ$ )	Minor axis amplitude ( $\text{ms}^{-1}$ )	Ellipse (+ve cyclonic)	Orientation ( $^\circ\text{N}$ )
$M_2$	0.360	286.3	-0.224	-0.62	57.4
$S_2$	0.114	95.1	-0.074	-0.65	63.8
$K_1$	0.035	201.7	-0.010	-0.29	288.3
$MS_f$	0.027	258.8	-0.005	-0.19	68.17
$O_1$	0.019	4.3	-0.009	-0.47	276.8
$M_4$	0.013	342.5	-0.001	-0.04	54.5

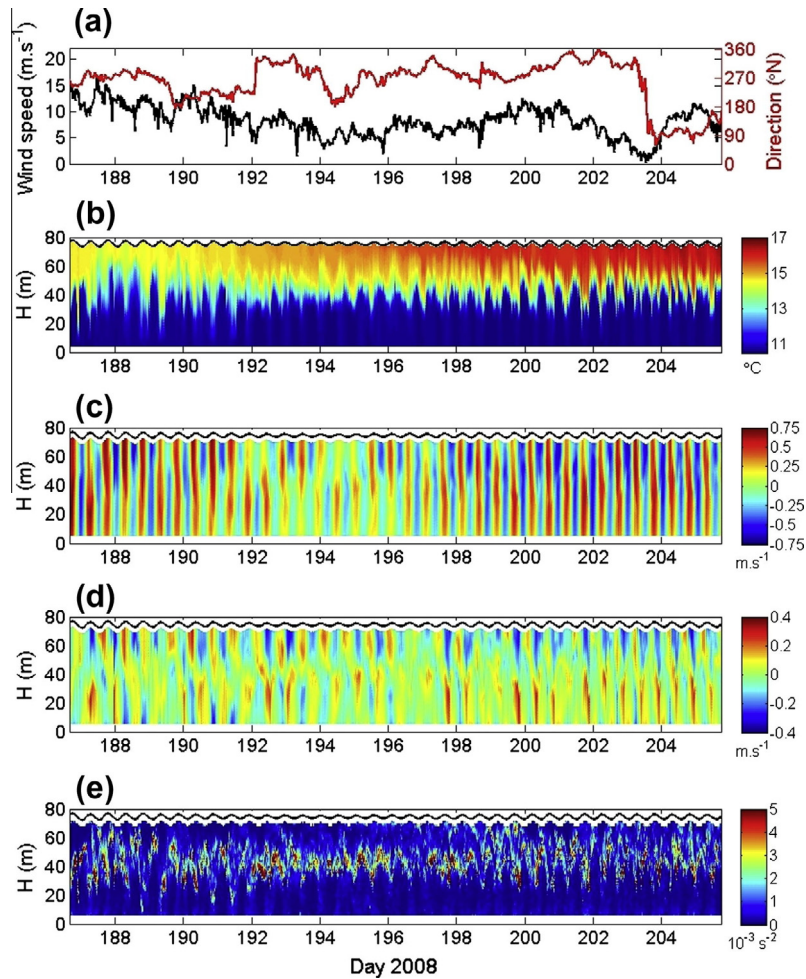


**Fig. 4.** (a) Wind speed and direction from ship measurements at Jones Bank. Near crest station (MS1), (b) temperature, (c) major axis velocity (+ve 60°N), (d) major axis baroclinic velocity and (e) vertical shear in horizontal flow squared,  $S^2 = (\delta u/\delta z)^2 + (\delta v/\delta z)^2$ .

periods. There is however a clearly distinguishable difference between thermocline activity during the *stormy spring* (up to day 192) and *calm spring* (day 198 onwards); during the stormy spring period these transitions or *jumps* are fairly irregular in both timing and magnitude however during the second spring period these features become more regular and appear well aligned with tidal currents. Thermocline displacement (low pass filtered to 1 h) is closely associated with depth mean major axis flow ( $R^2 = -0.62$  compared to  $R^2 = -0.47$  during the stormy spring period). The negative correlation identifies that downward thermocline displacements

are associated with positive flow upstream (or down-slope) of MS1. The tight relationship between flow and thermocline displacements and rapid transitions in thermocline depth suggests local generation of hydraulic jumps generated by the interaction of stratified tidal flow with the bank (Nash and Moum, 2001; Brickman and Loder, 1993). Power spectra of thermocline displacements (Fig. 5) at MS1 identify a strong oscillation at the local inertial and the diurnal frequencies during the *stormy spring* and a relatively weak semi-diurnal ( $M_2$ ) oscillation when compared to the *calm spring* period, comparable in magnitude to the following neap tide.

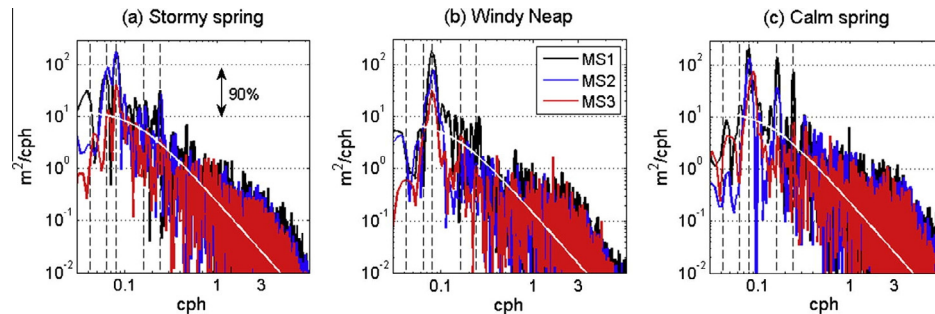


**Fig. 5.** Power spectra of vertical perturbations of the thermocline (represented by the average temperature) at sites MS1 (black), MS2 (blue) and MS3 (red) during the 3 different forcing states (a) to (c). The five vertical lines (left to right) indicate  $K_1$ , local inertial,  $M_2$ ,  $M_4$  and  $M_6$  frequencies. The slope of the idealised Garrett and Munk (1975) spectrum is shown for comparison (white). Typical 90% confidence limits are indicated in (a). (For interpretation of the references to color in this figure legend, the reader is referred to the web version of this article.)

Baroclinic energy (Fig. 4d) is high for the entire period with non-tidal velocities observed in excess of  $0.5 \text{ ms}^{-1}$  and rarely (1% of the time) less than  $0.1 \text{ ms}^{-1}$  at some point in the water column. As a result, a strong and narrow band of vertical shear in horizontal velocity is associated with the strongly stratified thermocline (Fig. 4e). While a strong shear layer is maintained throughout the time series the three different forcing states have a clear and dramatic effect on its vertical and temporal distribution, a result that appears strongly correlated to the dominant frequencies affecting the thermocline. Shear during the *stormy spring* is patchy and spread over large vertical ranges but strongest during peaks and troughs of low frequency internal waves. Beyond the tidal and sub-tidal frequencies that dominate thermocline displacement there is a broad distribution of energy over a higher frequency waveband between the  $M_2$  and  $M_6$  tidal constituents that continue into the windy neap period (Fig. 5b).

During the neap period (days 192–198) the shear layer is more consistent and associated with a less mobile thermocline oscillating at a tidal frequency, identifiable as a well defined isolated  $M_2$  peak in thermocline spectra (Fig. 5). During the '*calm spring*' period (days 198–206) we observe an energetic internal wavefield dominated by low frequency ( $M_2$ ) mode 1 baroclinic waves. Additional energy is observed in thermocline displacement spectra over the same range as during the stormy period however rather than a broadband spread of energy, clearly identifiable peaks are observed at the  $M_4$  and  $M_6$  frequencies. Internal waves with frequencies beyond the  $M_6$  tidal constituent are shown to follow the general structure of the idealised Garrett and Munk (1975) spectrum however there is some evidence of a contribution of energy from waves around the 1–3 cph waveband, close to the local buoyancy frequency, particularly evident during the calm neap period when the tidal frequency is dominant.

### 3.2.2. MS2: on slope station

The vertical structure of temperature at MS2 (Fig. 6) reveals a strong spring-neap modulation of the internal wavefield on the

bank slopes. As at MS1, the *stormy spring* period is clearly distinguishable from the remainder of the time series; maximum thermocline displacements are as high as 25 m and occasional rapidly occurring 'jumps' in isotherm depth are observed but the general character of the thermocline is irregular. Large jumps are observed periodically during the second spring phase when rapid displacements are observed in the thermocline associated with +ve off bank (+ve major axis) flow.

Although less energetic, there is a similar distribution of baroclinic energy throughout the time series to that at MS1; the stormy spring period produces large amplitude, predominantly low frequency displacements in the thermocline which are revealed by spectral analysis (Fig. 5) to be the combination of tidal and near inertial oscillations. Following this period, MS2 is dominated by the tidal frequency however unlike the near crest site there is no broadband spread of energy over the higher frequencies. During the second spring period peaks are again well described by the  $M_2$  and  $M_4$  frequencies although the  $M_6$  constituent is no longer significant. Beyond the distinctive tidal waveband (i.e.  $M_2$  to  $M_6$  frequencies) high frequency waves are slightly weaker in amplitude but otherwise have a similar distribution to MS1 and deviate from the canonical GM spectrum to indicate an increase of energy over a high frequency waveband.

### 3.2.3. MS3: off bank station

There is a marked decrease in baroclinic energy at MS3 when compared to the near crest and on slope stations (Figs. 5 and 6). The off-bank station occasionally experiences an increase in internal wave activity, again most commonly following spring tide, off-bank flow, but there are none of the large internal waves or jumps observed at the shallower sites during the spring periods and the ubiquitous internal tide, indicated by an  $M_2$  thermocline oscillation, is significantly weaker during all forcing scenarios. It is evident from both temperature data and thermocline displacement spectra that baroclinic energy dramatically diminishes with distance from the bank crest.

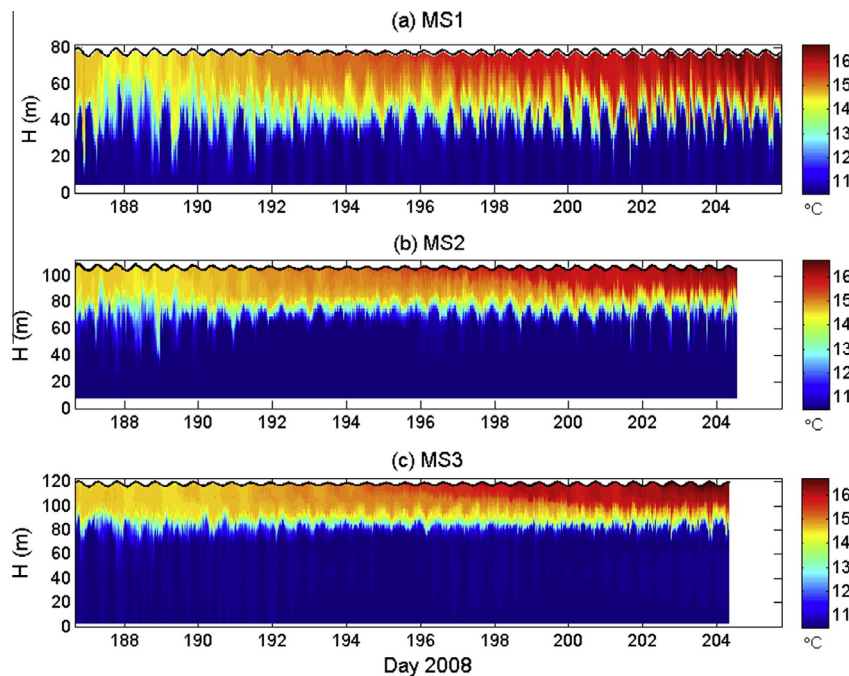


Fig. 6. Temperature chain data from a) the near crest site MS1, (b) the on slope site MS2 and (c) the off-bank site MS3 shows a decreasingly energetic internal wavefield with distance from the bank crest.

### 3.3. Internal waves and shear

Throughout all of our observations at Jones Bank the water column is strongly stratified and a strong shear layer exists in the thermocline due to disparity in horizontal flow between surface and bottom mixed layers. While some of this shear is attributable to high frequency internal waves it is the low frequency oscillation in these layers that makes the largest contribution to shear as is evident in the baroclinic velocity (Fig. 4d). The two most likely forcing mechanisms are the tides, both barotropic and a baroclinic internal tide, and inertial oscillations triggered by wind driven surface currents. The contribution to flow from tidal and inertial frequencies was identified by complex demodulation (Palmer et al., 2008) of the measured velocity at MS1. Due to the close proximity of the local inertial and  $M_2$  frequency at European latitudes a 3 day window was required to confidently separate the two constituents. This window is however insufficient to separate the  $M_2$  and  $S_2$  components therefore the spring neap modulation of the tide (Fig. 7a) is evident in what should otherwise be a constant  $M_2$  contribution. While weaker than the barotropic tide, inertial currents are significant with a magnitude in excess of  $0.15 \text{ ms}^{-1}$  at the start of the time series, reducing steadily with time until reaching a minimum at the calm period centred on day 203. While the relative phase of the tidal current remains unchanged with depth, as would be expected from barotropic forcing, the inertial current exhibits a  $180^\circ$  phase shift (not shown) above and below the thermocline consistent with previous shelf sea studies (e.g. Davies and Xing, 2005).

To examine the relative contribution to pycnocline shear from tidal and inertial forcing we examine the temporal change in bulk shear (Fig. 7b), calculated as the change in velocity between the surface mixed layer (sml) and bottom mixed layer (bml). The sml and bml were defined as the region bounded by  $0.1^\circ\text{C}$  below and above the surface and near bed temperature respectively. Bulk shear is highly variable and strongest during spring tide periods. During the calm spring period peaks are almost exclusively

observed following maximum +ve major axis flow, often ending abruptly around peak -ve minor axis flow towards the south-east. During the stormy spring period shear peaks are more sporadic, occurring on many different phases of the tide. During the neap tide period bulk shear variability is less dramatic and displays few of the peaks and troughs that characterise the more energetic periods, instead displaying a general decrease in magnitude between days 191 and 197. The bulk shear direction (Fig. 7c) identifies the dominance of the inertial component; shear follows the pathway of a predicted shear vector rotating at the local inertial frequency throughout the majority of the *stormy spring* period and almost exclusively during the neap phase, up to day 197. As inertial energy leaves the system there is a clear change in the characteristics of rotation until a transition occurs around day 197 when shear direction follows a pathway which becomes a mixture of significantly steeper and shallower rates of change, indicating shorter and longer period forcing respectively. Interestingly, none of the examples of shear vector which deviate from the inertial frequency have a semi-diurnal tidal frequency; the recurring steep sloping direction (a good example is day 200–200.3) has a rotational period equivalent to 9.8 h. The shallow sloping shear vector rotation that typically follows (e.g. day 200.3–200.6) has an equivalent period of between 25 and 40 h. The strongest bulk shear peaks (clearest examples are day 199.5 onwards in Fig. 7c) occur at the beginning of these shallow sloping periods. These slow moving shear events are short lived, typically lasting only 1–2 h, and always occur between  $280^\circ$  and  $360^\circ\text{N}$ , indicating the sml is west-north relative to the bml. The low shear values observed between peaks during the calm spring period are distributed over a broad range of directions.

### 3.4. Turbulence

Three time series of the dissipation rate of turbulent kinetic energy ( $\epsilon$ ), were collected at the slope station MS2 with the VMP, one during each of the three forcing states. Each period will

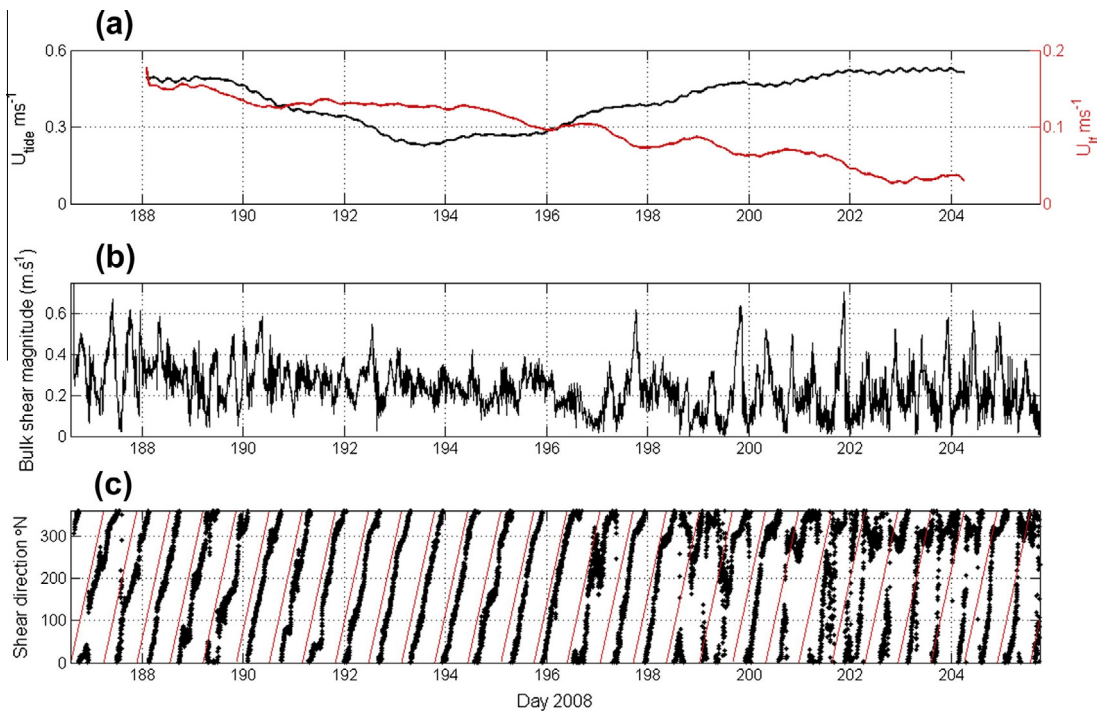


**Fig. 7.** (a) Tidal (black) and inertial (red) contribution to upper layer flow, note the different scales. (b) Bulk shear magnitude calculated as the rms vertical shear in horizontal velocity between upper and lower layers. (c) The bulk shear direction (black) is shown alongside the predicted progression of a purely inertial shear vector (red). (For interpretation of the references to color in this figure legend, the reader is referred to the web version of this article.)

now be examined separately in detail using nearby moored instrumentation to assist in the analysis. In each case the thermocline is defined as the region between 0.1 °C above near bed temperature and 0.1 °C below near surface values.

### 3.4.1. Stormy spring

Poor weather hindered operations considerably during the first of our microstructure time series and the need for other measurements not compatible with profiling (typically water sample collection for biological and chemical analysis) led to a number of gaps in data (Fig. 8e). Analysis of the vertical distribution of  $\varepsilon$  is still achievable however due to the strength of turbulent signatures during this period. VMP data were collected over a single tidal cycle (12.5 h) starting as the tidal current was increasing towards maximum +ve major axis flow, relative down slope at MS2. Current velocity was varied considerably with depth similar to coincident observations at the bank crest site MS1 (Fig. 8a–d). A strong shear layer was clearly evident at the pycnocline in both major and minor axes, strong enough to make upper and lower mixed layers identifiable as separately rotating layers. Particularly complex vertical current structures were evident around day 187.9 (Fig. 8c and d) when a strong ‘pulse’ of energy was observed in the major axis bml clearly distinguishable from tidal flow. During *off-bank* flow

isotherms are widely spread and show considerable variation with depth suggesting different layers within the pycnocline are under the influence of different forcing mechanisms. On the returning *on-bank* flow isotherms are more tightly spaced indicating a less diffuse, more stable pycnocline. The thermocline at MS1 follows a more dramatic path than at MS2 (Fig. 8a and b); similarly diffuse isotherms are observed during *off-bank* flow however the whole pycnocline appears controlled by the same mechanism/s indicated by highly correlated isotherm displacements. Each of the chosen isotherms decreases in height during *off-bank* flow before a rapid increase as +ve major axis flow decreases. As the tide turns, the pycnocline rapidly thins to 0 [10 m] and a rapid drop in depth of almost 30 m height is observed (day 187.95). Following this transition the thermocline returns to a more diffuse state similar to that at the start of our time series. Following the jump in isotherms at MS1 high frequency oscillations are evident in the velocity record indicative of propagating internal waves. Similarly, MS2 shows signs of increased high frequency internal wave activity during *on-bank* flow following the pulse of energy observed around day 187.9.

Measurements of  $\varepsilon$  (Fig. 8e) show high levels of turbulence throughout much of the water column and over the full tidal cycle however the strength of turbulent signatures permits identifica-

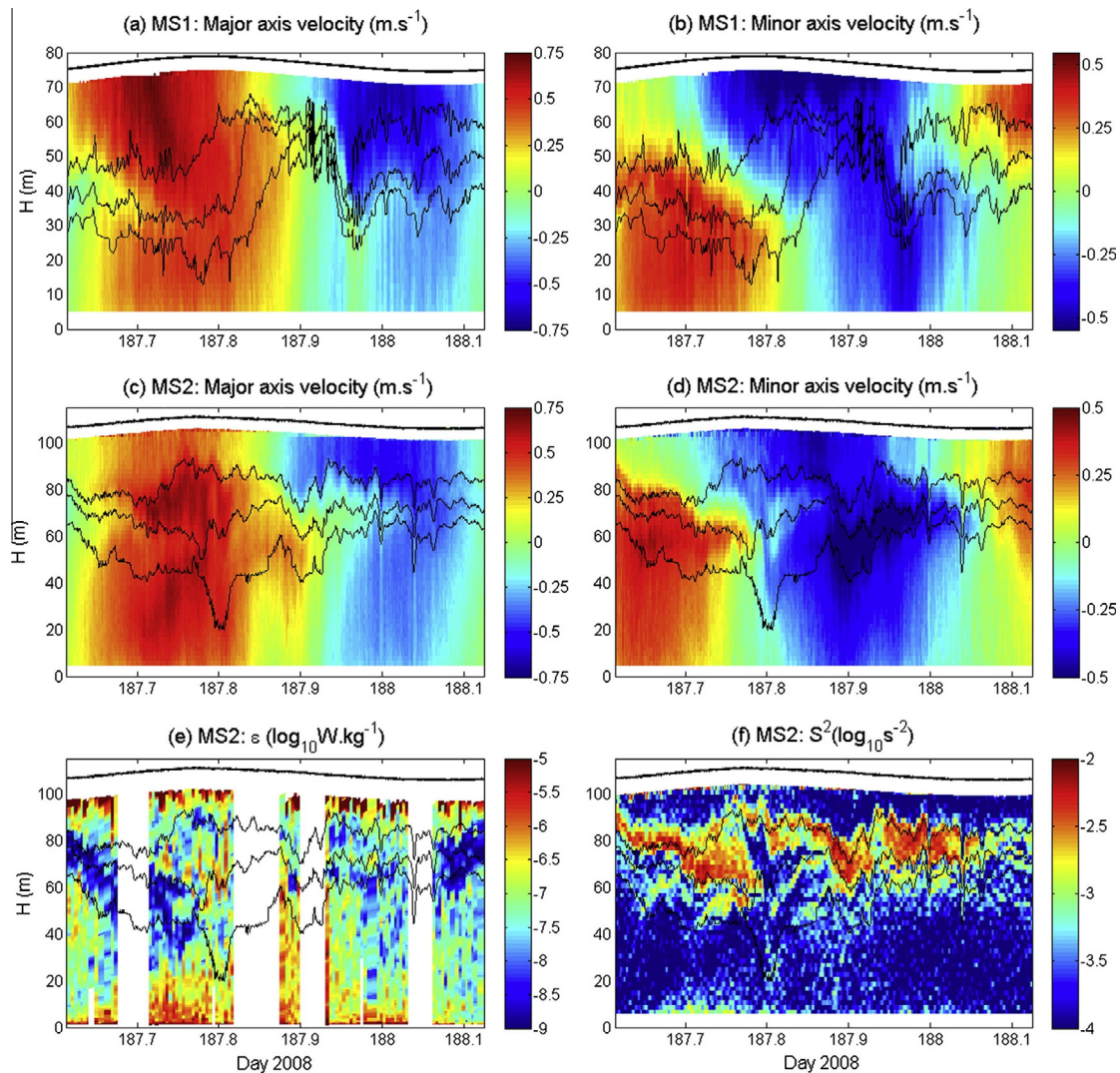


**Fig. 8.** Time series from the first series of microstructure measurements made during the stormy spring period, 6th–7th July 2008. (a) Major and (b) minor axis current velocity at MS1. The thermocline is indicated by 11, 12 and 13.5 °C isotherms (black lines). (c) Major and (d) minor axis currents at MS2. (e) Measurements of  $\varepsilon$  (2) and the (f) vertical shear in horizontal velocity,  $S$  are shown on a  $\log_{10}$  scale to identify the range of results over several orders of magnitude.

tion of separate mixing mechanisms. Surface mixing is intuitively high due to strong winds and decreases with distance from the sea surface.  $\varepsilon$  maintains levels 2–3 orders of magnitude above background levels throughout the sml and into the upper thermocline. At the base of the sml a strong shear layer is maintained throughout the majority of the tidal cycle (Fig. 8f) within which turbulence is highly variable. Within the pycnocline  $\varepsilon$  is patchy but does exhibit some evidence of layering; enhanced levels of turbulence are observed associated with strong shear layers, most notably around day 187.7–187.8 when a high shear region up to 20 m thick is associated with  $\varepsilon$  up to  $2 \times 10^{-6} \text{ W kg}^{-1}$  within a relatively diffuse pycnocline. A clearly distinguishable minimum in  $\varepsilon$  exists beneath this layer and the base of the pycnocline where energy levels are observed as low as  $5 \times 10^{-10} \text{ W kg}^{-1}$ , close to the detection limits of the VMP. Within the bml peaks in  $\varepsilon$  follow a typical quarter-diurnal response to tidal flow (Simpson et al., 1996) as turbulent kinetic energy is produced due to friction at the seabed and is rapidly dissipated; day 187.75 and 188.05 are associated with maximum *off-bank* and *on-bank* flow respectively. Separate from tidal maxima however there is a peak in  $\varepsilon$  associated with the previously identified *pulse* of major axis +ve velocity in the bml. While the vertical propagation of tidally associated  $\varepsilon$  varies over tidal time scales and weakens with height this pulse related peak in  $\varepsilon$  covers the entire bml up to the base of the pycnocline, 60 m above the seabed. This event, although poorly resolved, is preceded by an increase in height of the base of the thermocline of over 10 m at MS2. The event occurs approximately 1 h after a 30 m increase in isopycnals at MS1 and 1 h before a more rapid 30 m drop in isopycnal height at the near crest station. Isotherms are seen to broaden at MS2 and MS1 following these jump events, indicative of localised mixing, and there is evidence of a coincident increase in shear within the bml at MS2.

### 3.4.2. Windy neap

By comparison, the *windy neap* period is relatively quiet (Fig. 9). Throughout the single tidal cycle when turbulence measurements were made the pycnocline at MS2 maintained a fairly stable position. An internal tide of  $\sim 10 \text{ m}$  magnitude was evident and persistent short period, small magnitude internal waves were observed, typically exhibiting less than 10 m displacement. None of the jumps in isotherm height that characterised the previous spring period were observed. Turbulence at the surface and bed boundaries was weaker due to diminished wind and tidal mixing respectively. Bottom boundary layer turbulence is tidally driven and is contains insufficient energy to reach the thermocline. In the sml mixing is low with the exception of an increase during the latter stages of our measurements. The cause of this increase is unclear since there is no observed change in wind speed or direction. The night-time occurrence of this event suggests convective instability occurring as surface water cools, however observations fail to support this. High-resolution density profiles obtained simultaneously with shear microstructure provide no evidence of instability during this period, instead showing the surface to maintain a near surface temperature maximum throughout (Fig. 9d). Away from the boundaries there is a persistent layer at the base of the thermocline where  $\varepsilon$  is enhanced several orders of magnitude above the generally quiescent region that separates the pycnocline and the turbulent bottom boundary layer. Turbulence in this interfacial layer is patchy and typically  $O [10^{-8} \text{ W kg}^{-1}]$  although peak values are as high as  $3 \times 10^{-7} \text{ W kg}^{-1}$ . This peak occurs around day 195.7 when tidal flow was directed to the southeast. Unfortunately no current velocity data were available at MS2 during this period. Data from nearby MS1 however identifies strong mid-water shear in horizontal currents, identifiable as a vertical step change in horizontal velocity situated around the central isotherm.

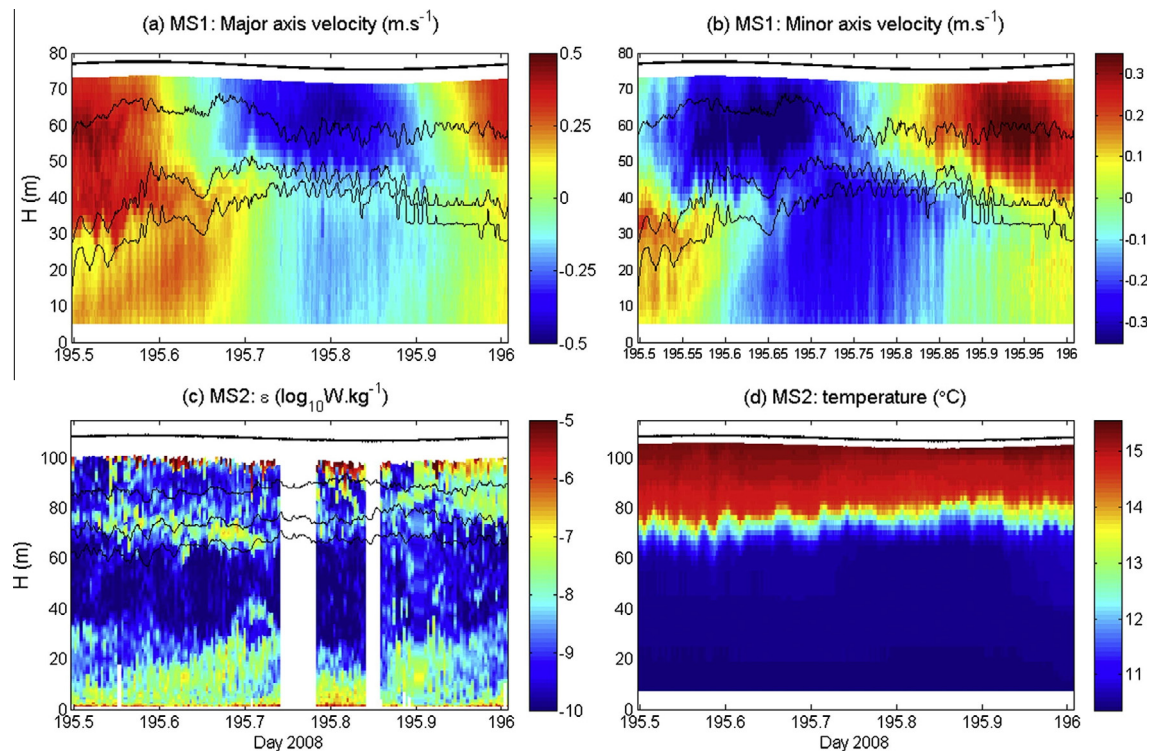


**Fig. 9.** Time series from the second microstructure period made during the windy neap, 14th–15th July 2008. Only ADCP data from the near crest station MS1 was available after failures at MS2 after 12th July. (a) Major and (b) minor axis current velocity at the MS1 is therefore shown to provide contextual support to data from MS2 data. The thermocline is indicated by 11, 13 and 15 °C isotherms (black lines). MS2 (c) measurements of  $\log_{10}\varepsilon$  (2) and (d) temperature structure from thermistor chain data.

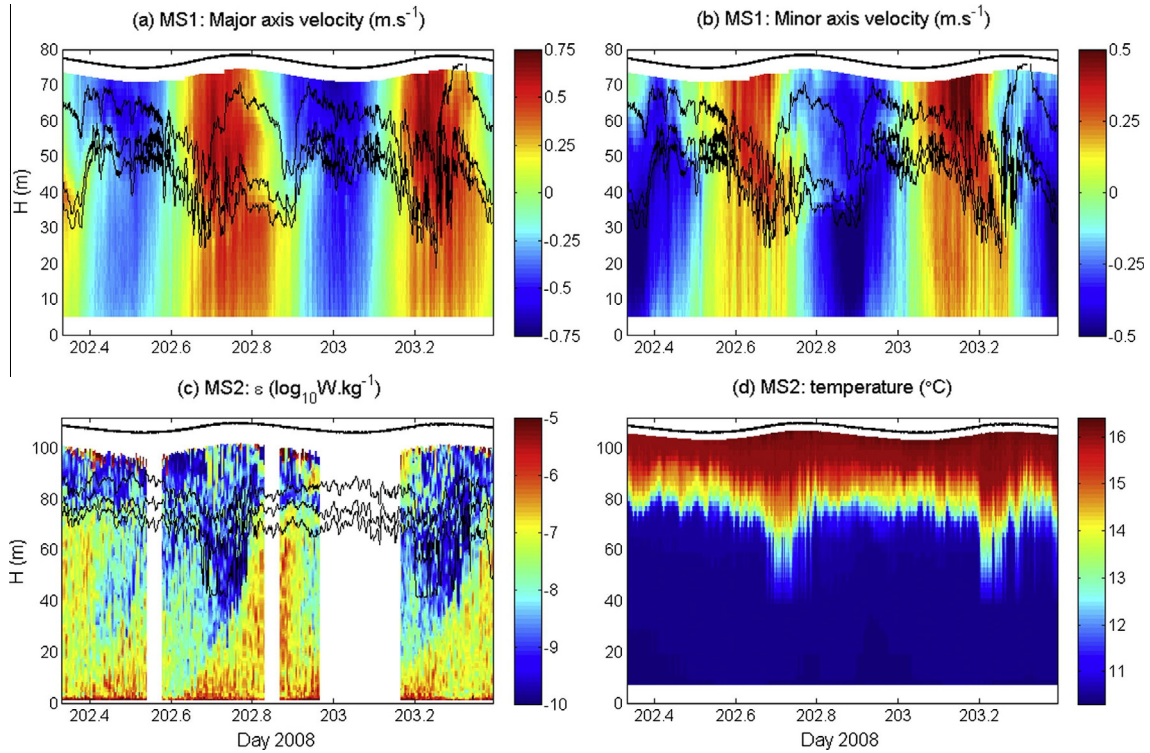


**Fig. 10.** Time series from the third microstructure series made over 2 tidal cycles during the calm spring period, 21st–22nd July 2008. As previously, only ADCP data from the near crest station MS1 was available. (a) Major and (b) minor axis current velocity at the MS1 is shown to provide contextual support to data from MS2 data. The thermocline is indicated by 11, 13 and 15 °C isotherms (black lines). MS2 (c) measurements of  $\log_{10}\epsilon$  (2) and (d) temperature structure from thermistor chain data.

### 3.4.3. Calm spring

The final microstructure time series was made over two tidal cycles during the *calm spring* phase (Fig. 10). The surface layer is predictably quiet although there is some evidence of night time surface mixing before and after the 2½ h break from profiling when the instrument tether unfortunately required repair. Tidally driven turbulence is clearly distinguishable in the bml, coincident with peak flow and exhibiting a phase lag with height above the seabed. Most striking however is a burst in  $\epsilon$  that stretches from the seabed to the base of the thermocline, elevating  $\epsilon$  in the bml as much as 4 orders of magnitude, up to  $10^{-6} \text{ W kg}^{-1}$ . Signatures of similar events are apparent at the beginning and end of the time series approximately one tidal period before and after the central event. The burst of energy in the bml occurs at a similar time as a highly energetic jump at the near crest site, identifiable by a swift transition in thermocline height and an abrupt change in bml velocity around day 202.9. Prior to this jump at MS1 there are a series of energetic internal waves associated with a depression in the thermocline at MS1 occurring during north-easterly, *off-bank* flow (i.e. day 202.7 and 203.2). This feature is repeated on the same phase of the following tide and is shadowed by tightly spaced packets of internal waves at MS2 shortly after.

### 3.5. Hydraulic jumps and elevated bed stress

The observed tidal association of thermocline displacements is indicative of the flow being under hydraulic control and the timing and rapidity that the thermocline position changes suggests the presence of hydraulic jumps (Farmer and Armi, 1999). Calculating the internal Froude number  $G^2$  (1) identifies the flow at the near crest site MS1 is regularly supercritical throughout both spring periods (Fig. 12a) when  $G^2$  is predominantly in phase with major axis current speed. By comparison, flow is predominantly subcritical during the neap period with only a few instances of near crit-

ical flow. Enhanced wind driven currents in the sml increase layer Froude number  $F_1$  dramatically during and following the *stormy spring* period. The thermocline at MS1 is regularly drawn down towards the seabed by supercritical flow in the bottom mixed layer associated with a flooding (+ve major axis) tidal flow. As the tide decreases following maximum flood hydraulic jumps are commonly observed, indicated by a sudden increase in thermocline height, and are associated with a transition from supercritical (or near supercritical) to subcritical flow in the lower layer at MS1. From the limited data available, bml flow at MS2 is never observed to become supercritical (not shown) suggesting that a transition in hydraulic state regularly occurs between the two sites during spring tides.

The tidal asymmetry of supercritical flow at the seabed at MS1 has important implications for turbulent bed stress,  $\tau_b$ , due to its quadratic relation with near bed velocity,  $U$ , since,

$$\tau_b = -\rho C_D |U|U \quad (4)$$

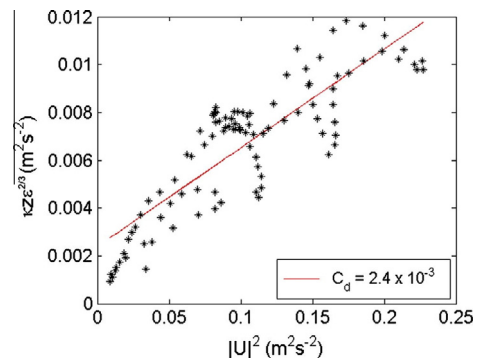


**Fig. 11.** The relationship between velocity (10 m above bed) and the turbulent bed stress provides an estimate of the local drag coefficient,  $C_D$ .

where  $C_D$  is the drag coefficient and represents the coupling between flow at the seafloor and flow away from the constant stress layer which covers only the first few metres of the water column. Our measurements of near-bed  $\varepsilon$  enables a local estimate of  $C_D$  to be made by comparing direct measurements of bed stress calculated from law-of-the-wall scaling of  $\varepsilon$  (Dewey and Crawford, 1988) and the observed flow at a reference layer, 10 m above the bed (Fig. 11).  $C_D$  at Jones Bank was calculated as 0.0024 in close

agreement to previous findings in shelf sea regions (e.g. Rippeth et al., 2002).

While a tidal oscillation is observed in bed stress along the major axis current direction (Fig. 12b) there is a clear asymmetry in the minor axis component associated with easterly supercritical flow (producing increased westerly  $\tau_b$ ) in the bottom mixed layer indicated by  $F_2$  close to or in excess of 1, particularly during the second spring phase, following day 197. Such flows only occur dur-

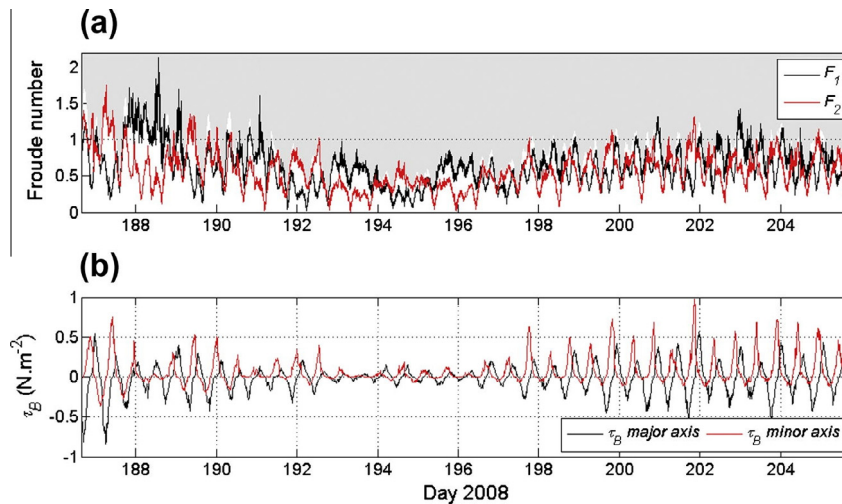


**Fig. 12.** (a) Upper (black) and lower (red) layer Froude number.  $F = 1$  is indicated by the dashed line and the unshaded region is  $G^2$  (2). (b) Major axis (black) and minor axis (red) component of  $\tau_b$  (4). (For interpretation of the references to color in this figure legend, the reader is referred to the web version of this article.)

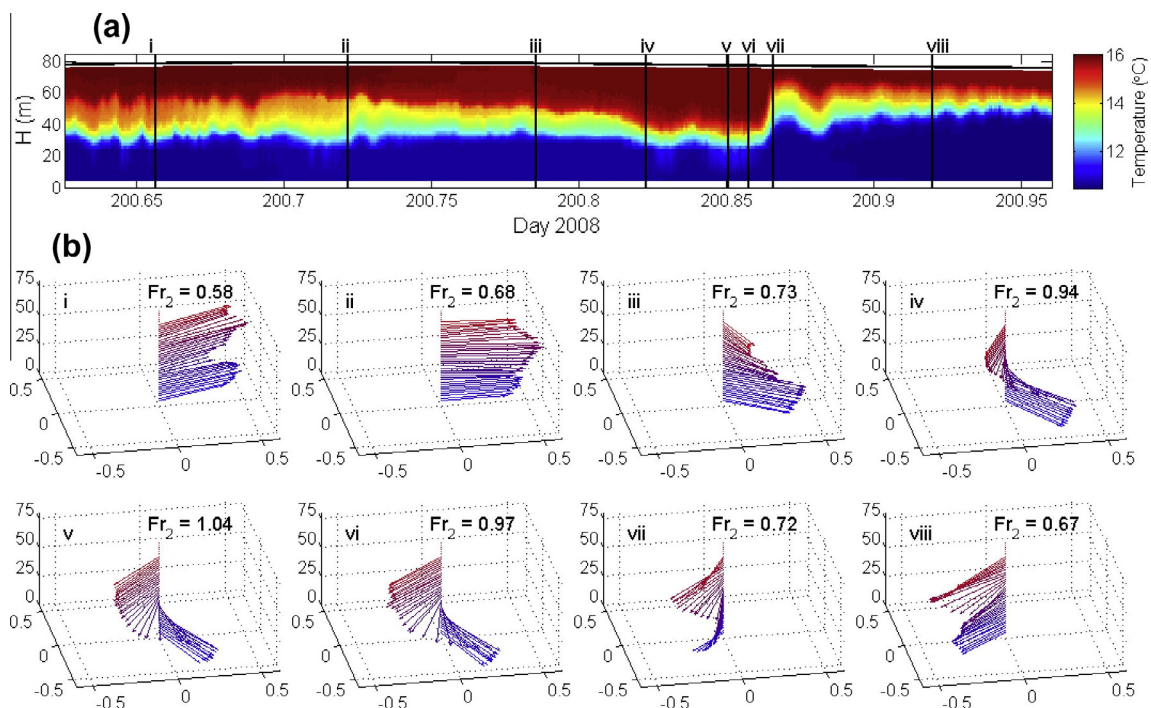


**Fig. 13.** The evolution of a hydraulic jump at Jones Bank is examined using the temperature chain data and vertical structure of velocity measured at the near crest site. Following maximum off bank major (red) axis flow the lower layer is seen to accelerate independently of the upper mixed layer. The flow is supercritical at this point (although the locally derived  $F_2$  is slightly less than 1); the lower layer is dominated by its kinetic energy which draws energy from the potential energy of the system. Bml flow is observed to increase and the thermocline is drawn downwards, reducing the thickness of the already intensified bml, increasing turbulent bed stress. Energy from the generated lee wave is free to propagate away from the bank but is prevented from travelling in the on-bank direction by the tide. Bml flow appears trapped at a critical angle in the south-easterly direction (iii–vi), bml flow direction typically being held within a  $20^\circ$  window for approximately 2 h. Flow is eventually ‘released’ during a sudden transition from super to subcritical flow and kinetic energy is released in the form of a hydraulic jump and broadening of the pycnocline. The bml then resumes a similar pathway to the sml. (For interpretation of the references to color in this figure legend, the reader is referred to the web version of this article.)

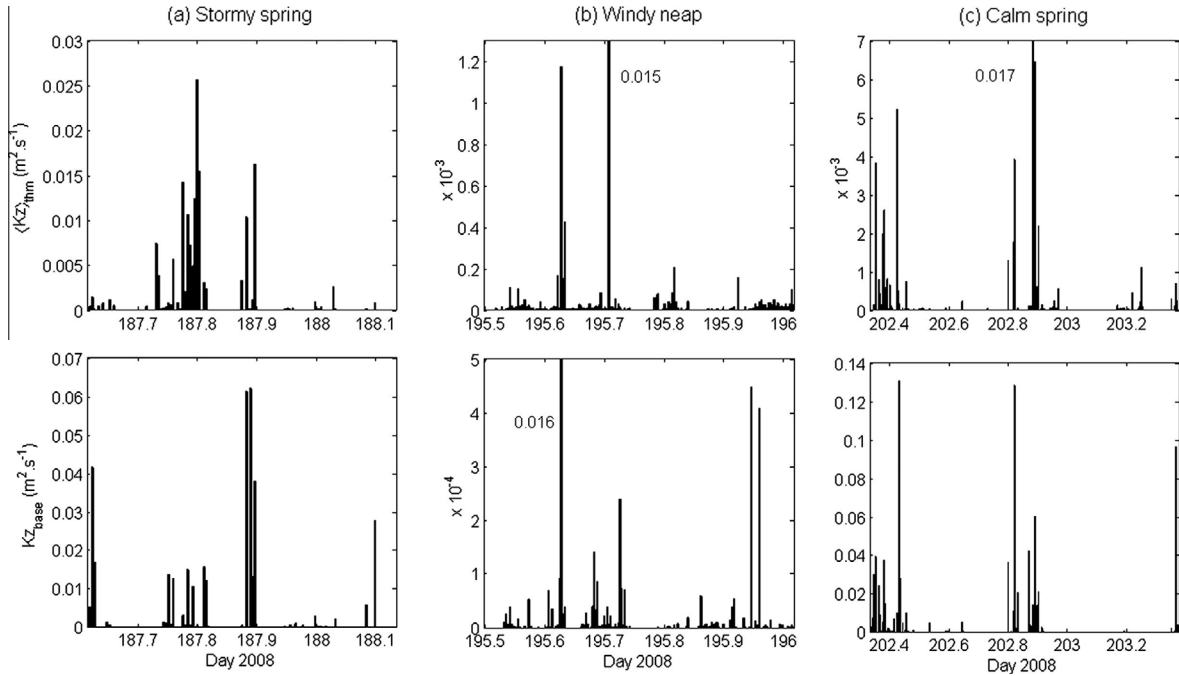


**Fig. 14.** Thermocline mixing at MS2 for (a) stormy spring, (b) windy neap and (c) calm spring periods. Upper panels show the average turbulent mixing rate (3) within the thermocline. Lower panels show the mixing rate at the base of the thermocline. Individual 'extreme' values that lie outside of the chosen axes have values indicated.

ing the spring tide periods. During the *calm spring* phase supercritical flow and subsequent peaks in  $\tau_b$  are regular and predictable, occurring between peak +ve major ( $\sim$ NE) and -ve minor axis ( $\sim$ SE) flow. During the windy spring period supercritical flow appears less orderly with the strongest contribution to  $G^2$  from the upper mixed layer. Peaks in bed stress however maintain a tight relationship with supercritical, easterly flow in the bml. Only relatively weak bed stress is experienced during the opposite phase of the tide at MS1. Jumps are observed whenever there is a rapid decrease in lower layer Froude numbers. The typical evolution of these regular features is presented in Fig. 13 which traces the horizontal flow at MS1 during one identified jump.

### 3.6. Vertical mixing

Dissipation rates (Figs. 8–10) in the bml are tidally dominated with additional increases associated with the observed bursts in  $\varepsilon$  assumed to result from nearby hydraulic jumps. Dissipation rates in the thermocline are highly variable but never exceed the energy levels observed in the bml. During the *stormy spring* period enhanced thermocline turbulence is observed during strong off-bank flow. During both spring periods, jump associated bursts of enhanced  $\varepsilon$  in the bml reach the thermocline typically increasing  $\varepsilon$  by 3 orders of magnitude above background levels at the base of the stratified region.

The mixing associated with the observed thermocline turbulence is now investigated in terms of the vertical eddy diffusion rate,  $K_z$  (3) (Fig. 14). During the stormy spring phase, strong shear driven mixing is observed in the thermocline coinciding with supercritical off bank flow and during the previously identified 'pulse' event ( $\sim$ day 187.9). The average measured thermocline mixing rate for this tidal period is  $1.9 (\pm 1.0^1) \times 10^{-3} \text{ m}^2 \text{ s}^{-1}$  although peak values are an order of magnitude higher. The base of the thermocline marks the interface between nutrient rich bottom water and the relatively stable environment of the shallow seasonal

thermocline. It is here that the jump event produces the strongest vertical mixing where a peak mixing rate of  $6.2 \times 10^{-2} \text{ m}^2 \text{ s}^{-1}$  is observed (Fig. 14a lower panel, day 187.91). During the neap tide period thermocline mixing is lower although strong sporadic mixing occasionally increases  $K_z$  to values comparable with spring tide events. The average measured thermocline mixing rate for this period is  $1.3 (\pm 1.3) \times 10^{-4} \text{ m}^2 \text{ s}^{-1}$ . Confidence levels in this value are clearly low since it is heavily influenced by 2 extreme values ( $1.2 \times 10^{-3}$  and  $1.5 \times 10^{-2} \text{ m}^2 \text{ s}^{-1}$ ) associated with short lived sporadic events. The timing of these peaks suggests they are associated with shear instability during off bank flow. Removing the 2 extreme values provides a more representative average thermocline mixing rate of  $2.8 (\pm 0.6) \times 10^{-5} \text{ m}^2 \text{ s}^{-1}$ . Mixing at the base of the thermocline is similarly low, typically  $O [10^{-5} \text{ m}^2 \text{ s}^{-1}]$  with the exceptions of a few sporadic increases and a single peak of  $1.6 \times 10^{-2} \text{ m}^2 \text{ s}^{-1}$ . During the *calm spring* period, average thermocline mixing increases significantly during each jump event but is otherwise relatively quiet. Average thermocline mixing rates for this period are  $3.3 (\pm 1.7) \times 10^{-4} \text{ m}^2 \text{ s}^{-1}$ . Thermocline mixing is dominated by jump related bursts of  $\varepsilon$  which is most felt at the thermocline base where mixing  $O [10^{-2} \text{ m}^2 \text{ s}^{-1}]$  regularly occurs and the strongest thermocline mixing rate measured at the bank is observed,  $1.6 \times 10^{-1} \text{ m}^2 \text{ s}^{-1}$ .

## 4. Summary

- The water over and around Jones Bank exhibits strong thermal stratification throughout the duration of our deployment even during gale and spring tide conditions.
- Stratified flow regularly interacts with Jones Bank sufficient to disturb the pycnocline to produce an internal tide observed over the extent of the bank and throughout the spring-neap cycle.
- During spring periods, major axis tidal current velocity is sufficient to produce crest-controlled supercritical flow in the bml. During *stormy spring* conditions, surface currents are sufficient to produce supercritical flow in the sml. During neap tides flow is almost entirely subcritical.

<sup>1</sup> Indicates 95% confidence limits based on bootstrap estimates of 200 samples.

- Baroclinic energy is seen to rapidly diminish with distance from the bank crest. Also, supercritical conditions are not observed in the bml at MS2 or MS3. This suggests baroclinic energy is lost close to the bank crest.
- Supercritical flow at MS1 produces regular hydraulic jumps generally occurring as flow passes over the flanks of Jones Bank, following peak off-bank flow. These flows also produce regular increases in local bed stress.
- High energy internal waves, supercritical flows and wind triggered inertial oscillations act to promote a persistently strong shear layer at the thermocline.
- Intense mixing is observed in the bml at MS2 during and following near-supercritical flow at the crest, not associated with tidally generated turbulence. Such mixing is observed as pulses of energy covering the whole of the bml and producing significant increases in  $K_z$  at the base of the thermocline.

## 5. Conclusions and discussion

Typical of much of the Northwest European shelf, the Celtic Sea is strongly stratified during summer months and experiences moderate to strong tidal flow. Wind and tide act to produce two distinct near surface and bottom mixed layers separated by a well defined temperature controlled pycnocline. During our three week experiment at Jones Bank in July 2008 the temperature difference between these two layers increased from 3.4 °C to 4.9 °C. Much of this increase is attributable to the recovery from storm conditions in the sml at the beginning of the experiment. The bml temperature remained near constant other than a small periodic fluctuation of 0.15 °C likely associated with the tidal advection of a patch of water from the bank crest indicative of locally increased levels of vertical mixing. Tidal flow over the bank is elliptical with the minor axis component of velocity typically half the magnitude of the major axis. Both the flow and temperature structure over Jones Bank are highly dynamic; an extremely active internal wave-field exists at the crest where maximum thermocline displacements are as much as half the 80 m water depth. There is a clear spring-neap modulation of internal wave activity with the most energetic waves generated during spring tides although baroclinic energy is always high at the near crest site MS1. Away from the crest, energy is rapidly diminished; internal waves are less frequent and smaller in magnitude. Despite this solitary waves or packets of internal waves are regularly observed on the bank slope at MS2 during spring tides and are associated with peak off bank (+ve major axis) flow. Occasional increases in weak internal wave activity are observed off bank at MS3.

The most dramatic features observed at the bank are a series of hydraulic jumps that regularly occur throughout both of the observed spring tide periods. Our observations at MS1 allow the evolution of such features to be described; during major axis off-bank flow the bml velocity becomes supercritical ( $F_2 > 1$ ). The flow is dominated by its kinetic energy which draws energy from potential energy in the system resulting in an increase in velocity and reduction in bml thickness. The subsequent 'drawdown' of the thermocline generates internal waves as energy is able to propagate away from the bank crest. During maximum supercritical flow the bml layer often appears trapped or stalled in a narrow 20° window for up to 2 h. The sml continues to follow the tidal elliptical path which results in an increase in thermocline shear as the layers are drawn apart, adding to the already strong shear layer, promoting instability. The mechanism behind the stalling of the bml flow is not clear but could be the result of topographic steering of a nearby indentation on the flanks of the bank (discussed later as a potential scour pit), enhanced bed stress or could be the result of competition between supercritical tidal flow and the return flow generated by the lee wave. When the bml is finally released in a

dramatic return to subcritical flow by way of a hydraulic jump, the bml returns to a more barotropic state, in phase with the sml.

While there were unfortunately no microstructure measurements made at the near crest site, the more diffuse nature of the thermocline at MS1 following each jump event (Figs. 8 and 10) is indicative of locally enhanced diapycnal mixing. Further down the slope at MS2 we observe intense mixing in the bml following off-bank major axis flow during all three of the spring tide cycles covered with VMP measurements. With a local buoyancy frequency  $N^2 \sim 1.5 \times 10^{-4} \text{ s}^{-2}$  and mean depth  $\sim 80$  m the estimated speed of a mode 1 internal wave at the crest is approximately  $1 \text{ ms}^{-1}$  (Gill, 1982). Assuming any energy from a hydraulic jump would propagate as an internal wave, we may draw some qualitative connection between the observed jumps observed at MS1 and the enhanced  $\varepsilon$  in the bml observed at MS2, since the horizontal distance between sites would take approximately 2.5 h to travel. We suggest that the energetic feature is the signature of a turbulent 'bore' generated by a hydraulic jump occurring between the two sites during maximum flow. This jump is visible in isotherm displacements in Fig. 10a at days 202.65 and 203.25 which precede the turbulent bore observed at MS2 by approximately 2.5 h. A similar feature at MS1 is observed on day 187.825; although poorly resolved due to interruptions to VMP profiling a turbulent bore is observed at MS2 approximately 1.5 h later.

Regularly enhanced bottom stress resulting from tidally asymmetric supercritical flow at MS1 is likely to have dramatic effects on the local topography. Enhanced flow will result in scouring and suspension of bed material while the rapid transition from supercritical to subcritical flow is likely to result in regular deposition of suspended sediment. Studies of hydraulic jumps in turbidity flows have identified regular deposition of sediments sufficient to maintain large scale features such as canyon fans on continental slopes (e.g. Kostic and Parker, 2006). It is possible that regular deposition of suspended material on Jones Bank will result in the development of step features on the bank slopes. Benthic studies undertaken during this experiment have identified that high energy areas such as MS1 support little fauna when compared to surrounding regions which is typical of scouring (personal communication, Nick Owen, Trinity College, Dublin). Close inspection of the local bathymetry shows evidence of small scale features of 1–3 km scale on Jones Bank slopes (Fig. 1b) and a feature similar to a scouring pit is visible on the flanks of the bank close to MS1. Such features may act to increase the likelihood of enhanced hydraulic flow due to steepening of the bank slope and changes to flow and/or layer thickness. There is potential therefore for a self maintaining mechanism where hydraulic flows lead to morphological changes which in turn lead to a greater likelihood of hydraulic jumps. The relationship between hydraulic jumps and long term bank morphology will be the focus of a future study.

Thermocline mixing at Jones Bank is dominated by hydraulic jumps during spring periods. Average thermocline mixing during the windy and calm spring periods is  $19 (\pm 10)$  and  $3.3 (\pm 1.7) \times 10^{-4} \text{ m}^2 \text{ s}^{-1}$  respectively. Average thermocline mixing during the neap period is  $1.3 (\pm 1.3) \times 10^{-4} \text{ m}^2 \text{ s}^{-1}$ , not significantly lower than during the calm spring measurements however confidence in this value to describe the typical mixing environment is clearly low indicated by the high confidence limits. Excluding two extreme values provides a typical neap background mixing rate of  $2.8 (\pm 0.6) \times 10^{-5} \text{ m}^2 \text{ s}^{-1}$ . High winds play an obvious role in increasing thermocline mixing during the first period (Fig. 8) but do little to increase mixing at the base of the thermocline which typically marks the strongest nutrient gradient and so is where vertical exchange is critical for sustaining biological growth in the stable environment of the summer thermocline and maintaining the SCM. During hydraulic jumps mixing rates at the base of the thermocline are intense; short lived peaks in mixing rates

regularly exceed  $10^{-2} \text{ m}^2 \text{ s}^{-1}$  with a maximum of  $1.6 \times 10^{-1} \text{ m}^2 \text{ s}^{-1}$ , 4 orders of magnitude greater than typical neap tide mixing rates.

This typical neap mixing rate is consistent with previous studies on shelf seas which find rates  $O [10^{-5} \text{ m}^2 \text{ s}^{-1}]$  (e.g. Palmer et al., 2008; Rippeth and Inall, 2002; Sandstrom and Oakey, 1995). The mechanism driving much of this mixing appears to be a persistent shear layer maintained by inertial oscillations. Studies at a nearby site, away from topographic features such as Jones Bank, by Palmer et al. (2008) found that inertial shear was sufficient to maintain a marginally stable thermocline, prone to destabilisation from relatively small inputs of additional shear from low energy internal waves. Our findings at Jones Bank provide further support to this theory. This is encouraging to the marine modelling community that seeks to better parameterize diapycnal mixing since the mixing associated with low mode, low frequency wavefields appears to scale well with local stratification and shear (MacKinnon and Gregg, 2003; Palmer et al., 2008). The challenge then remains to represent the locally generated mixing as described in this paper which, if accurate topography is available, may be within reach of current capabilities. We suggest however that the subtle role of small scale topography, such as that described in this study, requires further investigation.

Due to the strong nutrient gradient associated with the shelf sea seasonal pycnocline (Hickman et al., 2009; Sharples et al., 2001), the observed mixing events are likely to result in an injection of nutrients into an otherwise resource limited environment. We suggest therefore that the mechanism controlling the intensification of biological production over the bank, identified by the enhanced concentration of chlorophyll in the pycnocline, has been identified and explained; the relatively strong tidal flow of seasonally stratified water over Jones Bank during spring tides is sufficient to promote supercritical flow in the lower mixed layer resulting in the generation of a lee wave by hydraulic control, identifiable as a significant draw down of the pycnocline and an acceleration in current velocity during off bank flow. The waning tide triggers a transition from super to subcritical flow and a sudden release of energy in the form of a hydraulic jump. The mixing associated with this jump is sufficient to rapidly mix the lower layer and increase mixing in the base of the pycnocline where nutrient gradients are strongest. Due to the spring dependence of the observed mixing mechanism and identified relative stability of neap periods, the likelihood of biological assimilation of the enhanced nutrient supply is increased by providing alternating periods of strong mixing and stability.

### Acknowledgements:

We thank the officers and crew of the RRS James Cook and staff at NMFSS and NOC for their assistance in collecting the presented data. This work was funded under the UK Natural Environment Research Council Oceans2025 strategic marine science programme.

### References

Anderson, G.C., 1969. Subsurface chlorophyll maximum in the Northeast Pacific ocean. *Limnology and Oceanography* 14 (3), 386–391.

Armi, L., 1986. The hydraulics of two flowing layers with different densities. *Journal of Fluid Mechanics* 163, 27–58.

Brickman, D., Loder, J.W., 1993. Energetics of the internal tide on northern Georges Bank. *Journal of Physical Oceanography* 23, 409–424.

Carter, G.S., Gregg, M.C., Lien, R.C., 2005. Internal waves, solitary-like waves, and mixing on the Monterey bay shelf. *Continental Shelf Research* 25 (12–13), 1499–1520.

Davies, A.M., Xing, J., 2005. The effect of a bottom shelf front upon the generation and propagation of near-inertial internal waves in the coastal ocean. *Journal of Physical Oceanography* 35, 976–990.

Dewey, R.K., Crawford, W.R., 1988. Bottom stress estimates from vertical dissipation rate profiles on the continental shelf. *Journal of Physical Oceanography* 18, 1167–1177.

Elliott, A.J., Clarke, T., 1991. Seasonal stratification in the northwest European shelf seas. *Continental Shelf Research* 11 (5), 467–492.

Farmer, D.M., Armi, L., 1999. Stratified flow over topography: the role of small scale entrainment and mixing in flow reestablishment. *Proceedings of the Royal Society of London. Series A* 455, 3221–3258.

Fasham, M.J.R., Holligan, P.M., Pugh, P.R., 1983. The spatial and temporal development of the spring phytoplankton bloom in The Celtic Sea, April 1979. *Progress in Oceanography* 12 (1), 87–145.

Garrett, C., Munk, W., 1975. Space–time scales of internal waves: a progress report. *Journal of Geophysical Research* 80 (3), 291–297.

Gill, A.E., 1982. *Atmosphere–Ocean Dynamics*. Academic Press, Inc., 122.

Green, J.A.M., Simpson, J.H., Legg, S., Palmer, M.R., 2008. Internal waves, baroclinic energy fluxes and mixing at the European shelf edge. *Continental Shelf Research* 28, 937–950.

Hibiya, T., 1988. The generation of internal waves by tidal flow over Stellwagen Bank. *Journal of Geophysical Research* 93 (C1), 533–542.

Hickman, A.E., Holligan, P.M., Moore, C.M., Sharples, J., Krivtsov, V., Palmer, M.R., 2009. Distribution and chromatic adaptation of phytoplankton within a shelf sea thermocline. *Limnology & Oceanography* 54 (2), 525–536.

Holloway, P.E., Chatwin, P.G., Craig, P., 2001. Internal tide observations from the Australian North West shelf in summer 1995. *Journal of Physical Oceanography* 31, 1182–1199.

Inall, M.E., Aleynik, D., Neil, C., 2013. Horizontal advection and dispersion in a stratified shelf sea: the role of inertial oscillations. *Progress in Oceanography* 117, 25–36.

Ivey, G.N., Imberger, J., 1991. On the nature of turbulence in a stratified fluid. Part I: the energetics of mixing. *Journal of Physical Oceanography* 21, 650–658.

Kostic, S., Parker, G., 2006. The response of turbidity currents to a canyon-fan transition: internal hydraulic jumps and depositional signatures. *Journal of Hydraulic Research* 44, 631–653.

Lawrence, G.A., 1990. On the hydraulics of Boussinesq and non-Boussinesq two-layer flows. *Journal of Fluid Mechanics* 215, 457–480.

Lu, Y., Lueck, R.G., 1999. Using a broadband ADCP in a tidal channel. Part I: mean flow and shear. *Journal of Atmospheric and Oceanic Technology* 16, 1556–1567.

MacKinnon, J.A., Gregg, M.C., 2003. Mixing on the late-summer New England Shelf–Solibores, Shear and stratification. *Journal of Physical Oceanography* 33, 1476–1492.

Macoun, P., Lueck, R., 2004. Modeling the spatial response of the airfoil shear probe using different sized probes. *Journal of Atmospheric and Oceanic Technology* 21, 284–297.

Moum, J.N., 1996. Efficiency of mixing in the main thermocline. *Journal of Geophysical Research* 101 (C5), 12057–12069.

Moum, J.N., Nash, J.D., 2000. Topographically-induced drag and mixing at a small bank on the continental shelf. *Journal of Physical Oceanography* 30, 2049–2054.

Muller-Karger, F.E., Varela, R., Thunell, R., Luerssen, R., Hu, C., Walsh, J.J., 2005. The importance of continental margins in the global carbon cycle. *Geophysical Research Letters* (32), L01602.

Nasmyth, P.V., 1970. *Ocean Turbulence*. Ph.D. Thesis. University of British Columbia, 69 pp.

Nash, J.D., Moum, J.N., 2001. Internal hydraulic flows on the continental shelf: high drag states over a small bank. *Journal of Geophysical Research* 106 (C3), 4593–4612.

Oakey, N.S., 1982. Determination of the rate of dissipation of turbulent energy from simultaneous temperature and velocity shear microstructure measurements. *Journal of Physical Oceanography* 12, 256–271.

Osborn, T.R., 1980. Estimates of the local rate of vertical diffusion from dissipation measurements. *Journal of Physical Oceanography* 10, 83–89.

Palmer, M.R., Rippeth, T.P., Simpson, J.H., 2008. An investigation of internal mixing in a seasonally stratified shelf sea. *Journal of Geophysical Research*, 113, C12005. doi:10.1029/2007JC004531.

Pingree, R.D., Holligan, P.M., Mardell, G.T., 1978. The effects of vertical stability on phytoplankton distributions in the summer on the Northwest European Shelf. *Deep Sea Research* 25 (11), 1011–1016.

Pingree, R.D., Mardell, G.T., Cartwright, D.E., 1981. Slope turbulence, internal waves and phytoplankton growth at the Celtic Sea shelf-break. *Philosophical Transactions of the Royal Society A* 302 (1472), 663–682.

Pingree, R.D., Mardell, G.T., Holligan, P.M., Griffiths, D.K., Smithers, J., 1982. Celtic Sea and Armorican current structure and the vertical distributions of temperature and chlorophyll. *Continental Shelf Research* 1 (1), 99–116.

Pingree, R.D., Mardell, G.T., New, A.L., 1986. Propagation of internal tides from the upper slopes of the Bay of Biscay. *Nature* 321, 154–158.

Rippeth, T.P., 2005. Mixing in seasonally stratified shelf seas: a shifting paradigm. *Philosophical Transactions of the Royal Society, Series A* 323, 2837–2854.

Rippeth, T.P., Williams, E., Simpson, J.H., 2002. Reynolds stress and turbulent energy production in a tidal channel. *Journal of Physical Oceanography* 32, 1242–1251.

Rippeth, T.P., Inall, M.E., 2002. Observations of the internal tide and associated mixing across the Malin Shelf. *Journal of Geophysical Research* (107 C), 3028.

Rippeth, T.P., Palmer, M.R., Simpson, J.H., Fisher, N.R., Sharples, J., 2005. Thermocline mixing in summer stratified continental shelf seas. *Geophysical Research Letters*. <http://dx.doi.org/10.1029/2004GL022104>.

Sambrotto, R.N., Niebauer, H.J., Goering, J.J., Iverson, R.L., 1986. Relationships among vertical mixing, nitrate uptake, and phytoplankton growth during the spring bloom in the southeast Bering Sea middle shelf. *Continental Shelf Research* 5 (1–2), 161–198.

- Sandstrom, H., Elliott, J.A., 1984. Internal tide and Solitons on the Scotian shelf: a nutrient pump at work. *Journal of Geophysical Research* 89 (C4), 6415–6426.
- Sandstrom, H., Oakey, N.S., 1995. Dissipation in internal tides and solitary waves. *Journal of Physical Oceanography* 25, 604–614.
- Scourse, J.D., Haapaniemi, A.I., Colmenero-Hidalgo, E., Peck, V.L., Hall, I.R., Austin, W.E.N., Knutz, P.C., Zahn, R., 2009. Growth, dynamics and deglaciation of the last British–Irish ice sheet: the deep-sea ice-rafted detritus record. *Quaternary Science Reviews* 28 (27–28), 3066–3084.
- Sharples, J., Tett, P., 1994. Modelling observations of the seasonal cycle of primary productivity: the importance of short-term physical variability. *Journal of Marine Research* 52, 219–238.
- Sharples, J., Moore, C.M., Rippeth, T.P., Holligan, P.M., Hydes, D.J., Fisher, N.R., Simpson, J.H., 2001. Phytoplankton distribution and survival in the thermocline. *Limnology and Oceanography* 46 (3), 486–496.
- Simpson, J.H., Crawford, W.R., Rippeth, T.P., Campbell, A.R., Choek, J.V.S., 1996. The vertical structure of turbulent dissipation in shelf seas. *Journal of Physical Oceanography* 26 (8), 1579–1590.
- Tennekes, H., Lumley, J.L., 1972. *A First Course in Turbulence*. MIT Press, Cambridge, Mass.
- Tsunogai, S., Watanabe, S., Sato, T., 1999. Is there a “Continental Shelf Pump” for the absorption of atmospheric CO<sub>2</sub>. *Tellus, Series B* 51, 701–712.
- Tweddle, J.F., Sharples, J., Palmer, M.R., Davidson, K., McNeill, S., 2013. Enhanced nutrient fluxes at the shelf sea seasonal thermocline caused by stratified flow over a bank. *Progress in Oceanography* 117, 37–47.
- van Haren, H., 2000. Properties of vertical current shear across stratification in the North Sea. *Journal of Marine Research* 58, 465–491.